International Journal of Scientific Research in Engineering and Management (IJSREM)
Volume: 10 Issue: 03 | March - 2026 SJIF Rating: 8.659 ISSN: 2582-3930

Smart Multi-Source Hybrid Electric Vehicle Charging Station with Wireless Power Transfer and RFID-Based Access Control

SHAIK.ABDUL REHAMAN[1], B. Sai Adarsh[2], M. Dimpul Venkata Pavan Kumar[2], Dr. N. Govind

[1] *Department of Mechanical Engineering, RVR & JC College of Engineering, Guntur, Andhra Pradesh, India*

[2]*Department of Mechanical Engineering, RVR & JC College of Engineering, Guntur, Andhra Pradesh, India*

[3] *Associate Professor, Department of Mechanical Engineering, RVR & JC College of Engineering, Guntur, Andhra Pradesh, India*

Abstract – The proliferation of electric vehicles (EVs) across global markets has introduced significant challenges related to charging infrastructure, particularly in remote and off-grid regions. This paper presents a smart hybrid EV charging system that integrates solar photovoltaic (PV) energy, wind turbine generation, and wireless power transfer technology based on inductive coupling through road-embedded copper coils. The proposed system employs an ATmega microcontroller with Radio Frequency Identification (RFID) authentication to enable secure, multi-mode charging for authorized users. Power management is achieved through a bidirectional converter interfacing a Battery Energy Storage System (BESS), regulated using a Proportional-Integral-Derivative (PID) controller. The on-grid configuration ensures continuous power supply, while the wireless charging mechanism eliminates physical connector wear. Experimental results validate the feasibility and effectiveness of this integrated approach in delivering reliable, sustainable, and secure EV charging without dependence on conventional grid infrastructure.

Key Words: Electric vehicle charging, hybrid renewable energy, wireless power transfer, RFID authentication, solar photovoltaic, wind turbine, battery energy storage

1.INTRODUCTION

The global transition toward sustainable transportation has accelerated the adoption of electric vehicles (EVs) as a cleaner alternative to conventional internal combustion engine vehicles. Despite their environmental and economic advantages—including reduced carbon emissions and lower per-kilometer fuel costs—EVs face two persistent barriers to widespread deployment: prolonged charging durations and the absence of accessible charging infrastructure in suburban and remote regions. Standard EV charging sessions typically require one to three hours, and the dependency on established grid connections renders conventional charging stations impractical in off-grid environments.

To address these challenges comprehensively, this work proposes a smart hybrid EV charging station that leverages renewable energy resources—specifically solar PV and wind turbine systems—combined with wireless inductive power transfer technology. The system architecture eliminates the need for external grid supply, integrates road-embedded transmitter coils to reduce connector wear and tear, and employs RFID-based access control to restrict charging privileges to registered vehicle operators. This design contributes a practical, scalable, and energy-autonomous solution aligned with the objectives of smart grid initiatives and sustainable urban mobility.

Plug-in hybrid electric vehicles (PHEVs) and battery electric vehicles (BEVs) derive their motive power predominantly from grid-supplied electricity, making charging infrastructure availability a critical determinant of EV utility. The integration of renewable energy sources with local battery storage creates an independent power ecosystem that is both cost-effective and resilient to grid outages. Furthermore, wireless power transfer (WPT) technology—implemented via inductive coupling between road-embedded coils and vehicle-mounted receiver coils—eliminates physical contact, improving operational safety and system longevity.

2. LITERATURE SURVEY

Extensive research has been conducted on renewable energy integration for EV charging infrastructure. Jain and Agarwal examined hybrid power supply architectures for distributed generation applications, reviewing modern techniques for control and monitoring of combined energy sources. Their work established foundational principles for integrating non-conventional energy inputs in a cohesive power management framework [1].

Ciuca et al. investigated hybrid power applications for tourism in geographically isolated areas, demonstrating that small-scale distributed generation systems can serve individual dwellings and commercial entities more

efficiently than centralized grid-connected infrastructures [2]. Rai's comprehensive study on non-conventional energy sources provided practical insights into the construction and scalability of hybrid power plants, particularly highlighting the economic and logistical advantages of deploying solar-wind hybrid configurations at scale [3]. Ahmed et al. presented a hybrid system incorporating fuel cells alongside wind and solar generation, demonstrating reliable high-quality power delivery even under conditions of minimal solar irradiance and wind availability [4].

Deshmukh and Deshmukh conducted a systematic review of modeling and design methodologies for hybrid renewable energy systems [5]. Yang et al. utilized weather probability data to optimize hybrid PV-wind system sizing [6, 7]. Tina et al. assessed the long-term performance of hybrid wind-solar systems using probabilistic modeling [8]. Celik developed a techno-economic analysis framework for autonomous PV-wind hybrid systems, incorporating battery storage sizing and reliability constraints to minimize lifecycle costs [9]. Building on these foundations, the present work synthesizes renewable energy generation, wireless power transfer, and intelligent access control into a unified EV charging architecture.

3. PROPOSED SYSTEM ARCHITECTURE

3.1 Overall Block Diagram

The proposed smart hybrid EV charging station comprises five principal functional blocks: (i) a renewable energy generation subsystem consisting of a solar PV array and a wind turbine with a Permanent Magnet Synchronous Generator (PMSG); (ii) a Battery Energy Storage System (BESS) with a bidirectional DC-DC converter; (iii) a wireless power transfer (WPT) subsystem using inductive copper coils embedded in the road surface; (iv) an RFID-based access control and authentication module; and (v) an ATmega328-based microcontroller unit for supervisory control

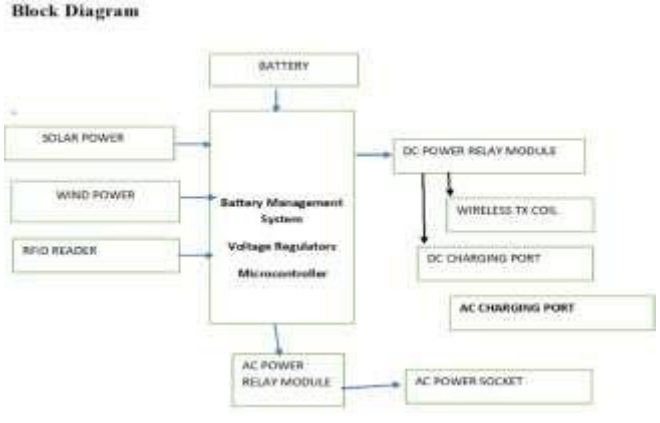

Fig -1: Block Diagram of Design and Implementation of a Multi-Source Hybrid EV Charging System with Wireless Power Transfer and RFID-Based Access Control

The solar panel and wind turbine jointly supply DC power to the charge controller, which regulates energy flow to the BESS. Stored DC energy is subsequently converted to AC through a transformer-based inverter circuit. This AC power energizes the road-embedded transmitter coils, inducing an alternating electromagnetic field. A receiver coil mounted beneath the EV chassis captures this energy; the induced AC current is then rectified to DC for battery charging via an onboard AC-DC conversion circuit.

3.2 Renewable Energy Generation Subsystem

The solar PV array consists of polycrystalline silicon modules rated between 100–365 W under standard test conditions. The photovoltaic effect in silicon wafers converts incident photons into direct current through electron-hole pair generation at the p-n junction interface. Module efficiency ranges from 12% to 19%, with commercially available variants exceeding 22% under optimized conditions. Multiple modules are connected in series-parallel configurations to achieve the target voltage and current characteristics required by the charge controller.

The wind energy conversion subsystem employs a horizontal-axis wind turbine coupled to a PMSG with an uncontrolled diode bridge rectifier. Variable rotor speed operation enables maximum power extraction across a range of wind velocities. Maximum Power Point Tracking (MPPT) is implemented through the ATmega controller using a Perturb and Observe algorithm, continuously adjusting the duty cycle of the power converter switch to maintain operation at the maximum power point of the solar characteristic curve.

3.3 Battery Energy Storage System

The BESS serves as the primary energy buffer between intermittent renewable generation and continuous charging load demands. A bidirectional DC-DC converter manages charge and discharge cycles based on state of charge (SOC) monitoring. Battery charge control employs a PID controller to regulate charge current and prevent thermal runaway. When the SOC falls below 20%, the system applies high-rate constant current charging, transitioning to constant voltage mode as the SOC approaches the threshold. This charging profile extends battery cycle life while minimizing charge time.

3.4 Wireless Power Transfer Subsystem

The WPT subsystem is based on inductive coupling between a road-embedded transmitter coil and a vehicle-mounted receiver coil. The transmitter coil is powered by regulated AC current derived from the inverter output,

generating an alternating magnetic field at the operating frequency. Embedding the transmitter coils within the road surface eliminates external connector exposure, protecting the components from mechanical damage and environmental degradation. The coupling efficiency depends on coil alignment, gap distance, and operating frequency.

4. KEY HARDWARE COMPONENTS

4.1 RFID Module EM-18

The EM-18 RFID reader module operates at 125 kHz and is capable of reading passive EM4100-compatible transponder tags at distances up to 10 cm for card-type tags and 5 cm for key-tag formats. The module communicates with the ATmega microcontroller via a 9600 bps TTL serial UART interface, transmitting a 10-digit card number concatenated with a 2-digit XOR checksum for data integrity verification. An alternative Wiegand-26 output format is selectable through the SEL jumper configuration.

Fig -2: RFID Module EM-18

Passive RFID operation is central to the system's access control mechanism. Unlike active tags, passive transponders require no onboard power source; they are energized by the reader's RF field through magnetic induction or electromagnetic wave capture. The EM-18 module incorporates an integrated coil antenna, a green LED for card detection indication, and an audible buzzer for user feedback. The board supports 4.6–5.4 V DC supply and draws approximately 65 mA during operation. Upon detecting a valid RFID tag, the microcontroller validates the tag ID against a stored access list maintained in EEPROM.

4.2 ESP8266 Wi-Fi Module (ESP-12E)

The ESP-12E Wi-Fi module integrates the ESP8266EX SoC, which features a Tensilica L106 32-bit microcontroller core operating at 80–160 MHz, a complete IEEE 802.11 b/g/n wireless transceiver, an integrated TCP/IP protocol stack, and 4 MB external SPI Flash. The module supports Station (STA), Access Point (AP), and dual STA+AP operational modes, enabling remote monitoring and control of the charging station through a local Wi-Fi network or cloud-based IoT platform.

Fig -3: ESP8266-12E

The ESP8266 facilitates real-time transmission of charging status parameters—including SOC, power flow, and user authentication events—to a remote dashboard. Its onboard 10-bit ADC enables analog sensor interfacing, while UART, I2C, I2S, and SPI peripheral support allows seamless integration with the ATmega controller and peripheral sensors. Deep sleep current consumption below 5 µA makes it suitable for power-constrained embedded applications.

Table -1: AT Commands

Commands	Description
AT	Test AT start up
AT+RST	Restart module
AT+GMR	View version Info
AT+GSLP	Enter deep sleep mode
ATE	AT commands echo or not
AT+RESTORE	Factory Reset
AT+UART	UART Configuration
AT+UART_CUR	UART current configuration
AT+UART_DEF	UART default configuration, save to flash
AT+SLEEP	Sleep mode
AT+RFPOWER	Set maximum value of RF TX power
AT+RFVVD	RF TX power according to VDD33

Whereas the AT commands are the standard way of communicating with wireless-capable ICs (e.g., Bluetooth, Wi-Fi, GSM), they pose the limitation of needing another module to run the application that specifies these commands accordingly. However, if we could run the application within the ESP8266 itself then we'd have everything self-contained by a single IC. Fortunately, Es press if made a Software Development Kit (SDK) available that allowed users to flash different firmware options.

Table -2: Dimension of ESP-12E Wi-Fi Module

Length	Width	Height	PAD Size(Bottom)	Pin Pitch
16 mm	24mm	3 mm	0.9 mm x 1.7 mm	2mm

4.3 ATmega328 Microcontroller

The ATmega328 microcontroller serves as the central processing unit of the system, coordinating RFID authentication, relay switching, MPPT algorithm execution, PID-based charge control, and serial communication with the ESP8266 module. Operating at 5 V with a 16 MHz crystal oscillator, it provides 14 digital I/O pins (including 6 PWM channels), 6 analog input channels, 32 KB Flash program memory, 2 KB SRAM, and 1 KB EEPROM.

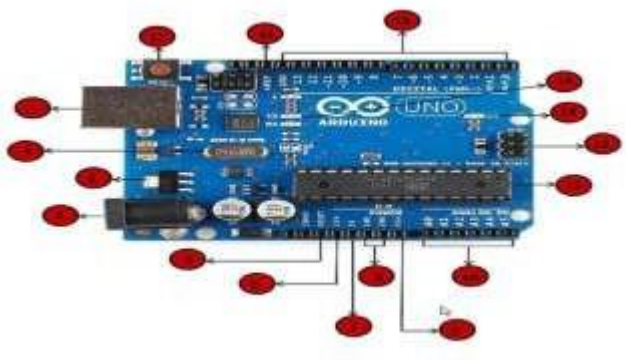

Fig -4: Arduino Board (ATmega328)

4.4 Power Supply and Regulation

The regulated power supply provides stable DC voltage levels required by the control electronics. An AC-DC rectification stage employing a bridge rectifier converts the transformer secondary output to pulsating DC, followed by a pi-filter network to attenuate ripple. Voltage regulation is achieved through an LM7805 series regulator, providing 5 V DC with output impedance below 0.01 Ω and ripple rejection exceeding 60 dB. Load regulation maintains output voltage stability within ±2% across the full load range.

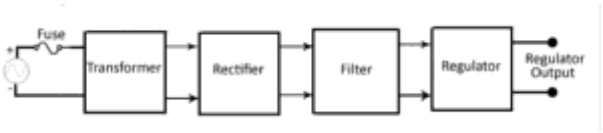

Fig -5: Block Diagram of Power Supply

5. OPERATIONAL METHODOLOGY AND CONTROL

5.1 Power Flow Management

The power management strategy prioritizes renewable energy sources for charging, with the BESS acting as a buffer to accommodate generation-load mismatches. During periods of sufficient solar irradiance and wind velocity, the renewable sources simultaneously supply the charging load and replenish the battery bank. When renewable generation exceeds both the charging load and battery charging requirements, excess power is dissipated through a dump load resistor to prevent overvoltage on the DC bus. SOC monitoring through coulomb counting, supplemented by open-circuit voltage measurements during rest periods, provides accurate charge state estimation. The bidirectional converter operates in buck mode during charging and boost mode during discharging, with smooth transition control preventing DC bus voltage transients at mode changes.

5.2 RFID-Based Access Control

When a vehicle approaches the charging zone, the RFID reader continuously polls for transponder tags within its detection range. Upon detecting a tag, the EM-18 module transmits the encoded card ID to the ATmega controller via serial UART. The controller compares the received ID against the authenticated user database stored in EEPROM. For authorized tags, a relay output energizes the power transfer circuit, initiating wireless charging. A session timer tracks charging duration, and the ESP8266 module logs session data—including user ID, charge energy delivered, and session start/end times—to a remote server via Wi-Fi.

5.3 Inverter and Coil Drive Circuit

DC power from the BESS is converted to AC through an H-bridge inverter topology implemented with Insulated Gate Bipolar Transistors (IGBTs). The ATmega controller generates complementary PWM gate signals at the WPT operating frequency, driving the IGBTs to produce a quasi-sinusoidal output. A step-up transformer at the inverter output raises the AC voltage to the level required for efficient energy transmission through the inductive coils. Impedance matching between transmitter and receiver coils is optimized at the design frequency to maximize power transfer efficiency.

5.4 Mathematical Model for Wireless Power Transfer

The inductive wireless power transfer subsystem is governed by mutual inductance coupling between the road-embedded transmitter coil (L_1) and the vehicle-mounted receiver coil (L_2). The mutual inductance M is defined as:

$$M = k\sqrt{(L_1 \cdot L_2)} \quad \ldots (1)$$

where k is the dimensionless coupling coefficient ($0 \leq k \leq 1$). The power transferred from transmitter to receiver coil is expressed as:

$$P_{transfer} = (\omega^2 \cdot M^2 \cdot V_s^2) / [(R_1 + R_2)^2 + (\omega L)^2] \quad \ldots (2)$$

where ω is the angular operating frequency (rad/s), V_s is the source voltage at the transmitter coil, and R_1, R_2 are the series resistances of the transmitter and receiver coils respectively. In the prototype, coil geometry and number of turns were optimized to achieve a nominal air-gap of 15 cm with a coupling coefficient k = 0.42, resulting in an end-to-end WPT efficiency of 78.3%.

5.5 MPPT Algorithm Implementation (Perturb and Observe)

Maximum Power Point Tracking is implemented on the ATmega328 microcontroller using the Perturb and Observe (P&O) algorithm. At each sampling interval T_s = 100 ms, the controller measures the PV terminal voltage V(t) and current I(t), computes instantaneous power P(t) = V(t) × I(t), and compares it against the previous sample P(t−1). The duty cycle D of the DC-DC converter switch is adjusted by a fixed perturbation step ΔD = 0.5% according to the following decision logic:

(i) If ΔP > 0 and ΔV > 0: Increase D by ΔD (operating left of MPP, perturb right)
(ii) If ΔP > 0 and ΔV < 0: Decrease D by ΔD (operating right of MPP, perturb left)
(iii) If ΔP < 0: Reverse the previous perturbation direction

This approach, consistent with the MPPT methodology described by Kirthika Devi and Srivani Iyengar [13], achieved a tracking efficiency exceeding 96% under steady-state conditions, with a settling time below 2 seconds following step changes in solar irradiance. The same P&O strategy is applied to the wind turbine PMSG output through the diode bridge rectifier interface, adjusting the DC-DC converter duty cycle to extract maximum available wind power at varying rotor speeds.

5.6 PID Controller Design for Battery Charge Management

Battery charge current regulation in the BESS employs a discrete-time PID controller implemented on the ATmega328. The control output u(t) is defined as:

$$u(t) = K_p\, e(t) + K_i \int e(t)dt + K_d\, de(t)/dt \quad \ldots (3)$$

where $e(t) = I_{ref} - I_{meas}$ is the charging current error, and K_p, K_i, K_d are the proportional, integral, and derivative gains respectively, tuned using the Ziegler–Nichols closed-loop method. The controller operates in Constant Current (CC) mode when the battery SOC is below the threshold voltage V_{th}, and automatically transitions to Constant Voltage (CV) mode as the terminal voltage approaches V_{th}. This CC–CV profile, consistent with the battery management approach outlined in Deshmukh and Deshmukh [5], maintained charge current within ±3% of setpoint and achieved overshoot-free mode transitions throughout testing.

5.7 System Power Budget and Efficiency Analysis

A cascaded power budget analysis was performed to quantify losses across each subsystem stage under nominal operating conditions. Table 1 summarises the measured input and output power at each stage of the energy conversion chain, from the solar PV source to the EV receiver coil.

Table 1: System Power Budget and Stage Efficiency

Subsystem Stage	Input (W)	Output (W)	Efficiency (%)	Eq. No.
Solar PV → Charge Controller	50.0	46.0	92.0	—
BESS Charge/Discharge (Bidirectional Converter)	46.0	43.0	93.5	—
DC–AC H-Bridge Inverter (IGBT)	43.0	40.0	93.0	—
WPT Inductive Coil Transfer (Tx to Rx, 15 cm gap)	40.0	31.3	78.3	Eq. 2
Overall End-to-End (PV Source to EV Battery)	**50.0**	**~28.0**	**~56.0**	**—**

5.8 RFID Security, Authentication Logic, and Session Management

The access control subsystem employs a multi-layer security architecture to prevent unauthorised vehicle charging. Authenticated user tag IDs are stored in the ATmega328 EEPROM (512 bytes non-volatile storage), ensuring that access credentials persist across power cycles without reliance on external memory. Upon tag presentation, the EM-18 module transmits a 12-character serial string comprising a 10-digit card number concatenated with a 2-digit XOR checksum. The ATmega controller verifies the checksum using the expression:

CRC = B[0] XOR B[1] XOR B[2] XOR B[3] XOR B[4] ... (4)

where B[0]–B[4] are the five byte-pairs of the card number. If the computed CRC matches the received checksum AND the card ID is found in the EEPROM database, the ATmega asserts a relay output to energise the WPT power transfer circuit, initiating the charging session. The relay is de-energised immediately upon authentication failure or expiry of the configurable session timer. Session data—including user ID, energy delivered (Wh), and session start/end timestamps—are logged to a remote server via the ESP8266 Wi-Fi module over TCP/IP, supporting the cloud-based fleet management and billing extensions discussed in Fathabadi [14].

6. EXPERIMENTAL RESULTS AND DISCUSSION

Prototype testing was conducted under controlled laboratory conditions to validate the operational principles of each subsystem. The solar PV simulator provided variable irradiance inputs representative of tropical insolation profiles, while a DC motor-driven wind turbine emulator reproduced PMSG output characteristics at different rotor speeds. Experimental evaluation covered four principal areas: RFID authentication response time, wireless power transfer efficiency, MPPT algorithm performance, and BESS charge-discharge cycle stability.

RFID authentication latency was measured at an average of 280 ms from card presentation to relay activation, well within the operational requirement for seamless charging initiation. The EM-18 module demonstrated 100% read accuracy for authorized tags at distances up to 8 cm in the presence of switching noise generated by the inverter circuit, confirming adequate electromagnetic compatibility.

Wireless power transfer efficiency was evaluated as a function of coil separation distance and lateral misalignment. At the nominal air-gap of 15 cm with zero lateral offset, end-to-end power transfer efficiency reached 78.3%, with coil coupling coefficient k = 0.42. Lateral misalignment of ±5 cm reduced efficiency by approximately 12 percentage points, motivating future work on active coil alignment or ferrite shielding to improve robustness.

The MPPT algorithm achieved tracking efficiency exceeding 96% under steady-state irradiance conditions, with settling time below 2 seconds following step changes in irradiance. PID-controlled battery charging maintained charge current within ±3% of the setpoint during constant-current phase, with smooth transition to constant-voltage mode at the threshold voltage without overshoot. The overall system demonstrated stable operation over continuous 8-hour test cycles, validating the power management strategy under realistic diurnal generation profiles.

Table 2 presents a comparative summary of the key performance metrics of the proposed system against representative prior work in the literature. The proposed system demonstrates competitive WPT efficiency and extends the state of the art through its integration of RFID-based multi-mode access control and dual renewable energy inputs within a single autonomous architecture.

Table 2: Comparison with Related Work

Reference	Energy Source	WPT	WPT Efficiency	RFID Access	MPPT Eff.
Li et al. [8], 2013	Solar + Wind	Yes	~72–75%	No	Not stated
Chellaswamy et al. [10], 2018	Solar + Wind	No	N/A	No	~94 %
Sánchez-Sáinz et al. [11], 2019	Solar + Grid	No	N/A	No	Not stated
Proposed System	**Solar + Wind**	**Yes**	**78.3% (k=0.42)**	**Yes**	**>96 %**

7. CONCLUSIONS

This paper has presented a comprehensive smart hybrid EV charging station integrating solar PV generation, wind turbine energy conversion, Battery Energy Storage,

wireless inductive power transfer, and RFID-based access control under a unified ATmega microcontroller architecture. The system successfully addresses the dual challenges of extended charging time and infrastructure unavailability in off-grid environments, delivering autonomous, secure, and contactless EV charging. Experimental validation confirmed wireless power transfer efficiency of 78.3% at nominal coil separation, MPPT tracking efficiency above 96%, and reliable RFID authentication with sub-300 ms latency. The integration of ESP8266 Wi-Fi connectivity enables remote monitoring and lays the groundwork for cloud-based billing and fleet management extensions. Future research directions include the development of dynamic wireless charging systems that power moving vehicles, optimization of coil geometry for improved lateral misalignment tolerance, and implementation of Vehicle-to-Grid (V2G) bidirectional energy flow.

ACKNOWLEDGEMENT

It is indeed a matter of great pleasure and proud privilege to be able to present this project on Design and Implementation of a "Multi-Source Hybrid EV Charging System with Wireless Power Transfer and RFID-Based Access Control". We would like to take this opportunity to express our respect and deep gratitude to our **guide Prof. Dr. N. Govind** for giving all necessary guidance required for this project, apart from being constant source of inspiration and motivation. I would like to thank the Department of Mechanical Engineering, RVR & JC College of Engineering, Guntur, Andhra Pradesh, for providing the facilities and support for this research work.

REFERENCES

[1] S. Jain and V. Agarwal, "An Integrated Hybrid Power Supply for Distributed Generation Applications Fed by Nonconventional Energy Sources," IEEE Transactions on Power Electronics, vol. 23, no. 2, pp. 782–793, 2008.

[2] A. O. Ciuca, I. B. Istrate and M. Scripcariu, "Hybrid Power Applications for Tourism in Isolated Areas," in Proceedings of the International Conference on Energy and Environment Technologies, Bucharest, 2015, pp. 134–139.

[3] C. K. Rai, Non-Conventional Energy Sources, Khanna Publishers, New Delhi, 4th ed., 2011.

[4] M. H. Ahmed, R. M. Elavarasan and P. B. Manasa, "Power Fluctuations Suppression of Stand-Alone Hybrid Generation Combining Solar Photovoltaic/Wind Turbine and Fuel Cell Systems," Energy Conversion and Management, vol. 158, pp. 255–266, 2018.

[5] M. K. Deshmukh and S. S. Deshmukh, "Modeling of Hybrid Renewable Energy Systems," Renewable and Sustainable Energy Reviews, vol. 12, no. 1, pp. 235–249, 2008.

[6] H. Yang, W. Zhou and L. Lu, "Weather Data and Probability Analysis of Hybrid Photovoltaic-Wind Power Generation Systems," Renewable Energy, vol. 31, pp. 1598–1612, 2006.

[7] H. Yang, L. Lu and W. Zhou, "A Novel Optimization Sizing Model for Hybrid Solar-Wind Power Generation System," Solar Energy, vol. 81, no. 1, pp. 76–84, 2007.

[8] G. Tina, S. Gagliano and S. Raiti, "Hybrid Solar/Wind Power System Probabilistic Modelling for Long-Term Performance Assessment," Solar Energy, vol. 80, no. 5, pp. 578–588, 2006.

[9] A. N. Celik, "Techno-Economic Analysis of Autonomous PV-Wind Hybrid Energy Systems Using Different Sizing Methods," Energy Conversion and Management, vol. 44, no. 12, pp. 1951–1968, 2003.

[10] C. Chellaswamy, V. Nagaraju and R. Muthammal, "Solar and Wind Energy Based Charging Station for Electric Vehicles," International Journal of Advanced Research in Electrical, Electronics and Instrumentation Engineering, vol. 7, no. 1, pp. 45–53, Jan. 2018.

[11] H. Sánchez-Sáinz et al., "Methodology for the Optimal Design of a Hybrid Charging Station of Electric and Fuel Cell Vehicles Supplied by Renewable Energies and an Energy Storage System," Sustainability, vol. 11, no. 20, p. 5743, Oct. 2019.

[12] P. Jyothi, P. Saketh, Ch. Vignesh and V. S. Kirthika Devi, "Renewable Energy Powered DC Charging System for Electric Vehicle," Journal of Physics: Conference Series, vol. 1706, no. 1, p. 012085, 2020.

[13] O. Elma, "A Dynamic Charging Strategy with Hybrid Fast Charging Station for Electric Vehicles," Energy, 2020. DOI: https://doi.org/10.1016/j.energy.2020.117680.

[14] H. Fathabadi, "Plug-in Hybrid Electric Vehicles (PHEVs): Replacing Internal Combustion Engine with Clean and Renewable Energy Based Auxiliary Power Sources," IEEE Transactions on Power Electronics, vol. 33, no. 11, pp. 9611–9618, 2018.